frontiers | Frontiers in Physics

BRIEF RESEARCH REPORT
published: 27 April 2022
doi: 10.3389/fphy.2022.851838

Abnormal Magnetoresistance Transport Properties of van der Waals Antiferromagnetic $FeNbTe_2$

Bao-tao Qi[1†], Jun-Jie Guo[1†], Ying-qing Miao[1], Mian-zeng Zhong[1,2], Bo Li[3], Zi-yan Luo[1], Xi-guang Wang[1], Yao-zhuang Nie[1], Qing-lin Xia[1,2] and Guang-hua Guo[1]*

[1]Hunan Key Laboratory of Nanophotonics and Devices and Hunan Key Laboratory of Supermicrostructure and Ultrafast Process, School of Physics and Electronics and State Key Laboratory of Powder Metallurgy, Central South University, Changsha, China, [2]Zhejiang Province Key Laboratory of Quantum Technology and Device, Zhejiang University, Hangzhou, China, [3]College of Semiconductors (College of Integrated Circuits), Hunan University, Changsha, China

The emergence of two-dimensional (2D) van der Waals magnetic materials has attracted enormous attention due to their novel physical phenomena and potential application in the fields of spintronics and information storage technology. Here, we systematically study the magnetic and transport properties of a van der Waals antiferromagnetic material, $FeNbTe_2$. The magnetic and magnetoresistance measurements verified its antiferromagnetic properties, spin glass state, and negative magnetoresistance effect at lower temperatures. In addition, the measurement results of transport also show the existence of angle-dependent anisotropic magnetoresistance in a wide temperature range and anisotropic magnetoresistance inversion in a certain temperature range.

Keywords: $FeNbTe_2$, chemical vapor transport, magnetoelectric transport properties, anisotropic magnetoresistance, magnetic properties

OPEN ACCESS

Edited by:
Xiao-Ping Wei,
Lanzhou Jiaotong University, China

Reviewed by:
Xiangrong Wang,
Hong Kong University of Science and Technology, Hong Kong SAR, China
Badih A. Assaf,
University of Notre Dame, United States

****Correspondence:***
Qing-lin Xia
qlxia@csu.edu.cn

†These authors have contributed equally to this work

Specialty section:
This article was submitted to Condensed Matter Physics, a section of the journal Frontiers in Physics

Received: *10 January 2022*
Accepted: *28 March 2022*
Published: *27 April 2022*

Citation:
Qi B-t, Guo J-J, Miao Y-q, Zhong M-z, Li B, Luo Z-y, Wang X-g, Nie Y-z, Xia Q-l and Guo G-h (2022) Abnormal Magnetoresistance Transport Properties of van der Waals Antiferromagnetic FeNbTe$_2$. Front. Phys. 10:851838. doi: 10.3389/fphy.2022.851838

INTRODUCTION

Two-dimensional (2D) layered materials with magnetic behavior (both ferromagnetic and antiferromagnetic) have received considerable attention in recent years because of their unique properties and potential application in spintronics and information storage technology [1–4]. The magnetic properties of intrinsic magnetic 2D layer materials can be tuned *via* van der Waals engineering, electrostatic gating, and strain engineering [5–9]. The magnetic properties of intrinsic nonmagnetic 2D can be introduced through the formation of vacancies or defects, adsorption of atoms, and doping transition metal atoms or nonmetal atoms [10–13].

Anisotropic magnetoresistance (AMR) effect, which is defined as magnetoresistance changes with an angle between magnetization and current [14], first reported by William Thomson [15], has been used in many fields like magnetic sensors and AMR-magnetic random-access memory (MRAM) devices [16]. The physical mechanism is very complicated, as stated in Refs. [17, 18]. Traditionally, AMR can be explained by spin-orbit coupling. If the direction of the magnetic field is perpendicular to the current, then the electronic orbits are parallel with the current and lead to a small cross-section for scattering, which results in a low resistance state. On the contrary, while the direction of the magnetic field is parallel to the current, the electronic orbits are perpendicular to the current, and the cross-section for scattering is larger, resulting in a high resistance state [19]. In recent studies of many new materials, such as Nb_3SiTe_6 [20], Dirac semimetal Cd_3As_2 [21], topological type-II Weyl semimetal like WTe_2 [22], and A-type antiferromagnetic $NaCrTe_2$ [23],

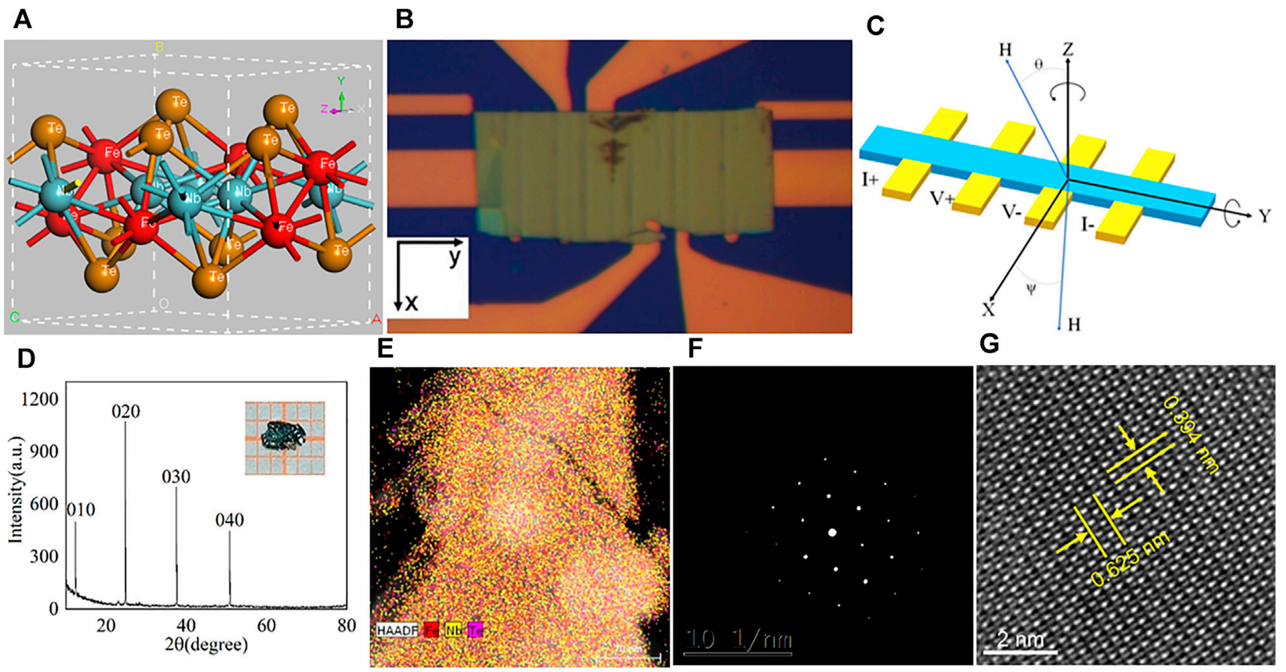

FIGURE 1 | (A) Diagram of the $FeNbTe_2$ unit cell and the lattice position of magnetic elements Fe with red balls. **(B)** Optical image of $FeNbTe_2$ micro-nano device; electrodes are parallel to each other. The size of the film is about 80 μm · 30 μm. **(C)** Schematic of the experimental configuration for anisotropic magnetoresistance on the xy and yz planes, respectively. **(D)** XRD pattern of $FeNbTe_2$ single crystal. The inset shows the optical image of the $FeNbTe_2$ crystal. **(E)** EDS mapping of three kinds of elements: Fe, Nb, and Te. **(F,G)** SADE and HRTEM images of $FeNbTe_2$ crystal.

this rule has been broken. The low resistance state exists when the applied fields are parallel to the current.

$FeNbTe_2$ is a 2D layered material with intralayer ferromagnetism and interlayer antiferromagnetism [24]; Jing Li et al. synthesized $FeNbTe_2$ single crystals and studied the transport properties. The research shows that $FeNbTe_2$ has a space group of *Pmna* (No. 53, **Figure 1A**), and its resistance increases with decreasing temperature, showing semiconductor characteristics. A detailed study on the magnetic properties of polycrystalline $FeNbTe_2$ was conducted by Jian H. Zhang et al. in 1997 [25]. The measurement χ_{ac} $(= dM/dH)$ confirms the existence of a spin glass state in the polycrystalline $FeNbTe_2$ sample with a transition at $T_f = 44$ K. The most recent study was reported in 2019 [26]. Chong Xiao et al. made $FeNbTe_2$ flake micro-nano devices and performed magnetoelectric transport measurements. They demonstrated an intrinsic unsaturated negative magnetoresistance (nMR) of $FeNbTe_2$. Angle-resolved photoemission spectroscopy (ARPES) measurement, the electronic transport measurement, and DC/AC magnetic susceptibility prove that the existence of intrinsic unsaturated nMR is due to the comprehensive effect of Anderson localization and a spin glass state. In this article, we systematically studied the anisotropic magnetoresistance of synthetic $FeNbTe_2$ single crystals.

METHODOLOGY

$FeNbTe_2$ single crystals were synthesized by a chemical vapor transport (CVT) process [24, 26]. All reagents, iron (99.99%), niobium (99.99%), and tellurium (99.99%) were purchased from Aladdin (Shanghai, China). The materials were mixed in a molar ratio of 1:1:2 and sealed in a 16-mm Δ 150-mm vacuum quartz tube, and 10 mg of iodine was used as a transport agent. In a two-temperature zone tube furnace, the sealed vacuum quartz tube was heated to 850°C (high temperature zone) and 750°C (low temperature zone) for 12 h, kept for 10 days, and then cooled to room temperature in 12 h. The structure of $FeNbTe_2$ single crystals was characterized by an X-ray diffractometer (XRD, Advance D8). To investigate the elemental composition and crystal structure, transmission electron microscopy (TEM) measurements were performed, in which the elemental composition was given by energy-dispersive spectrum (EDS) mapping, and the crystal structure was detected by selected-area electron diffraction (SAED) and high-resolution TEM (HRTEM).

Magnetic and transport measurements were performed in a Quantum Design Physical Property Measurement System with a 9 T magnet (PPMS-9T). The magnetic properties of the bulk sample were measured by using a vibrating sample magnetometer (VSM) integrated into the PPMS-9T with an accuracy of 10^{-7} emu. The resistivity of the thin flake on its (x, y) plane was measured by the standard four-terminal method, with a rotator sample holder for controlling the relative orientation between the magnetic field and the crystal. The $FeNbTe_2$ material was prepared into micro-nano devices for transport measurement. The device was prepared by transferring $FeNbTe_2$ flake onto the Au (50 nm)/Cr (5 nm) electrodes as

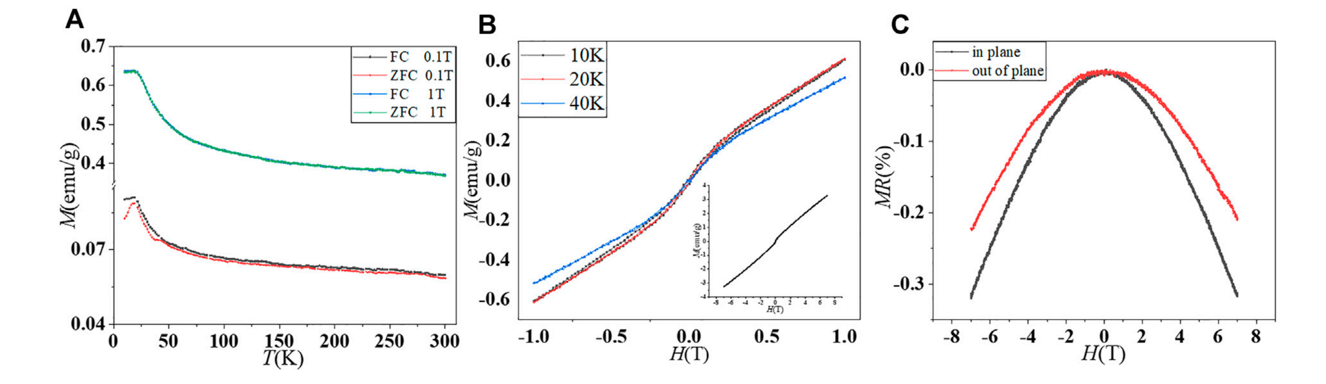

FIGURE 2 | (A) ZFC–FC magnetization curves of $FeNbTe_2$ versus temperature, measured at fields of 0.1 and 1 T. **(B)** Magnetization versus applied field up to 1 T for $FeNbTe_2$ at various temperatures 10, 20, and 40 K. The inset shows the magnetization versus applied field up to 7 T at 10 K. **(C)** nMR in both out-of-plane and in-plane applied magnetic field (*H*) at 10 K.

shown in **Figure 1B**, in which the flake was mechanically exfoliated from the single-crystalline bulk sample. Au (50 nm)/Cr (5 nm) electrodes were fabricated onto 285 nm SiO_2/Si substrates by using a standard ultraviolet radiation photolithographic procedure. As shown in **Figure 1C**, a standard rectangular coordinate system is established on the flake, with the flake plane as the *xy* plane. The *y*-axis is parallel to the current direction, the *z*-axis points to the normal direction of the sheet surface, and the *y*-axis is perpendicular to the *xz* plane. The angular dependence of MR was measured by rotating the sample in the magnetic field; θ and ψ are defined as the angle between the magnetic field and the z axis on the *yz* plane, and the magnetic field and the x axis on the *xy* plane, respectively, as shown in **Figure 1C**.

RESULTS AND DISCUSSION

The quality of the $FeNbTe_2$ single crystal was characterized by XRD, which is shown in **Figure 1D**. The sharp diffraction peaks and the (0*l*0) peaks show the interlaminar orientation of the single crystal along the b axis. The optics image of a $FeNbTe_2$ crystal is shown in the inset, the size is about 3 mm × 1.5 mm. The TEM characterization results are as follows: energy-dispersive spectra (EDS) mapping of elementals Fe, Nb, and Te is shown in **Figure 1E**. The distribution of the three elements is uniform, and the stoichiometric ratio of Fe, Nb, and Te is close to 1: 1: 2, consistent with the composition of the $FeNbTe_2$ crystal. The single-crystalline structure is further confirmed by selected-area electron diffraction (SAED) and high-resolution TEM (HRTEM), as shown in **Figure 1F** and **Figure 1G**. SAED shows clear spots, which demonstrates the single crystal nature of the $FeNbTe_2$ nanoplate. The HRTEM in **Figure 1G** image displays distinct lattice fringes with interplanar spacings of 0.394 and 0.625 nm, which are assigned to the orthorhombic $FeNbTe_2$ with lattice parameters of a = 0.792 and c = 0.624 nm [24].

Figure 2A shows the measured zero field cooled (ZFC) and field cooled (FC) temperature dependence of magnetization in an applied field of 0.1 to 1 T. With a field of 1 T, the ZFC–FC curves overlap with each other, which is quite different from the date, measured under 0.1 T. At an applied field of 0.1 T, when the temperature is higher than 22 K, the ZFC and FC magnetization decreases monotonically with the increase in temperature. When it is below 22 K, a distinct λ-shaped bifurcation appears between the two curves of ZFC and FC, which is generally considered one of the characteristics of spin glass [11]. **Figure 2B** displays the magnetization of $FeNbTe_2$ versus magnetic field H up to 1 T, measured at different temperatures. The curve measured at 10 K is similar to the curve at 20 K, which corresponds to the 22 K bifurcation point mentioned earlier. The coercivity H_C is ≈ 100 Oe at 10 K and decreases to ≈60 Oe at 20 K. At a higher temperature of about 40 K, the M–H curve behaves in a more paramagnetic linear correlation [27]. The magnetic moment saturation cannot be observed in a magnetic field up to 7 T at 10 K, as shown in the inset of **Figure 2B**.

To investigate the magnetic transport properties, the *MR-H* measurements were performed at 10 K with the magnetic field parallel to the *x*-axis and *z*-axis, respectively. As shown in **Figure 2C**, *MR* is normalized to the zero-field value R_0 by$MR(\%) = (R(H) - R_0)/R_0 \times 100\%$; the magnetoresistance decreases with increasing field, which is typically nMR. The value of nMR at 10 K under 7 T is ≈ −0.32%, consistent with previous reports [26]. It can also be seen that, compared with the rate of change with the magnetic field parallel to the *x*-axis, the *MR* measured with the magnetic field parallel to the *z*-axis is smaller.

When the magnetic field is applied along the *z*-axis and *x*-axis, the value of nMR differs by 30%; this shows the existence of anisotropy in this sample. The magnetic anisotropy of the $FeNbTe_2$ was investigated by angle-dependent magnetic resistance measurements; the magnetic field rotates along the *y*-axis and *z*-axis.

We first consider the AMR measurement with the magnetic field rotating within the *xz* plane. Here, two kinds of measurements were performed, one is the measurement of the angle-dependent magnetoresistances with a fixed magnetic field (9 T) at different temperatures, and the other is the measurement with different magnetic fields at isothermal conditions of 10 K. The results are normalized by$MR(\%) = (R - R(\theta = 0))/R(\theta = 0) \times 100\%$, as shown in **Figure 3A** and **Figure 3B**, respectively.

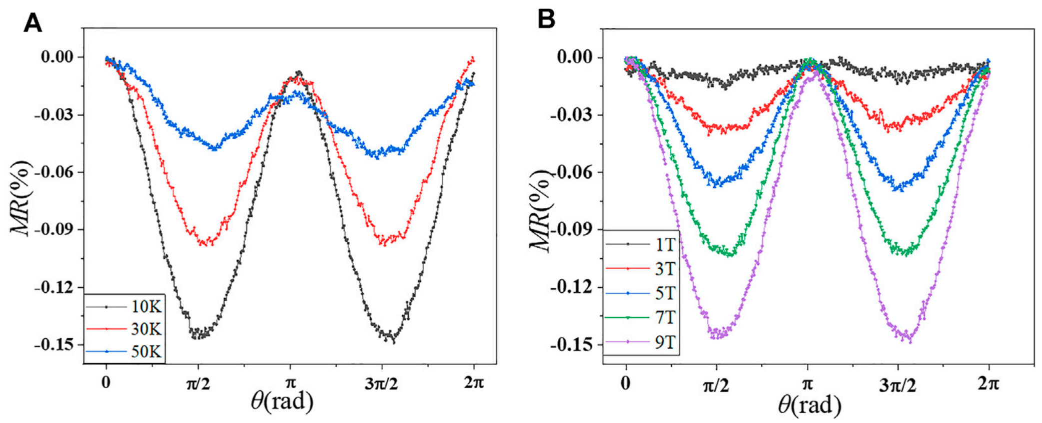

FIGURE 3 | (A) Out-of-plane AMR measured at 9 T at different temperatures. **(B)** Out-of-plane AMR at 10 K under different magnetic fields.

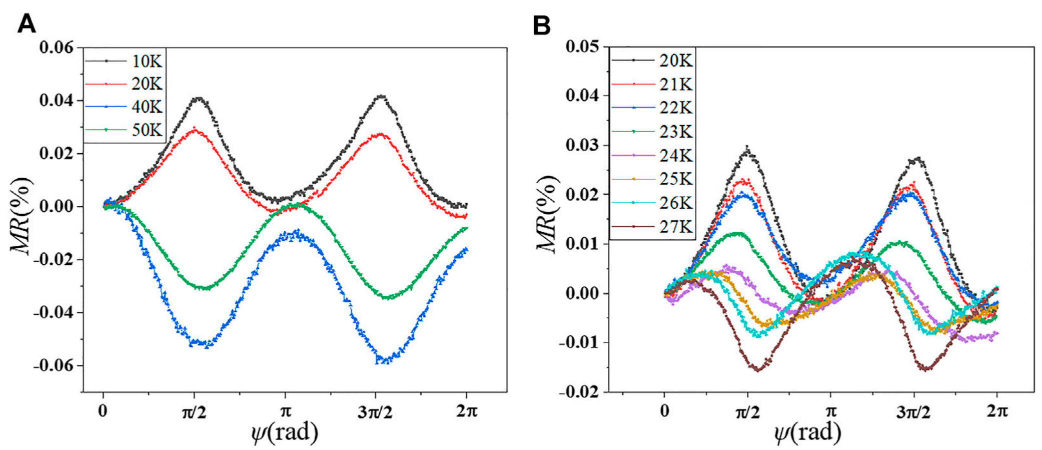

FIGURE 4 | (A) In-plane AMR at different temperatures: 10, 20, 40, and 50 K. **(B)** In-plane AMR between 20 and 27 K.

In **Figures 3A, B**, the MR curves take on a similar shape to a cosine square function of θ. The curve can be fitted with the formula$MR = -R_m cos^2(\theta + \pi/2)$. It can be seen from the figures that, under different conditions, the resistance when $\theta = 0$ is higher than the resistance when $\theta = \pi/2$. This is contrary to the principle of the traditional AMR [14, 15], while is similar to that of some new materials, Nb_3SiTe_6, Dirac semimetal Cd_3As_2, topological type-II Weyl semimetal WTe_2 and A-type antiferromagnet $NaCrTe_2$ [20–23]. As can be seen in **Figure 3A**, $FeNbTe_2$ flake shows obvious out-of-plane anisotropy up to 50 K, the anisotropic *MR* is about 0.14% at 10 K, and gradually decreases with increasing temperature. At a temperature of 10 K, the AMR is obvious under different magnetic fields. The AMR increases nearly linearly with the magnetic field increase, which is shown in **Figure 3B**.

Next, we consider the AMR measurement at different temperatures with the fixed magnetic field of 9 T and rotating within the *xy* plane. The normalized results are displayed in **Figure 4A** and **Figure 4B**. As shown in **Figure 4A**, the measurement was performed at temperatures ranging from 10 to 50 K. Different from the law of out-of-plane anisotropy; the variation amplitude of in-plane anisotropy is not strictly temperature-dependent. The temperature where the largest variation appears is about 40 K, with an amplitude of about 0.06%, and the curve flipped between 20 K and 40 K. At temperatures of 10 and 20 K, when the magnetic field is applied parallel to the *x*-axis, $\psi = 0$ rad, the resistance is minimum, and when $\psi = \pi/2$, the resistance is maximum, which is consistent with the spin-orbit coupling induced density of states and spin-related anisotropic scattering characteristics. When the magnetic moment is perpendicular to the direction of the current, the orbit of electronics is parallel to the direction of the current and is in a low resistance state, and when the magnetic moment is parallel to the direction of the current, it is in a high resistance state [28]. When the temperature rises to 40 K, the measurement curve is flipped along the *y*-axis, and the resistance is maximum when the magnetic field direction is perpendicular to the current. The curves can be fitted by the formula $MR = \mp R_m cos^2(\psi + \pi/2)$.

In view of the inversion of the curve within the temperature range of 20–27 K, a detailed measurement is carried out. As shown in **Figure 4B**, the curve gradually reverses as the temperature increases, and the reversal phenomenon is more obvious at the temperature of 24 K, which is close to the measured critical temperature of 22 K of the spin glass state of the sample. The reverse phenomenon may be attributed to the fierce competition between the ferromagnetic and antiferromagnetic states near the critical temperature of the spin glass state.

CONCLUSION

In short, we have explored the AMR properties of the $FeNbTe_2$ single crystal in this article. The measured results show that the out-of-plane AMR is contrary to the principle of the traditional AMR and is related to the intralayer ferromagnetic and interlayer antiferromagnetic configuration (A-type antiferromagnet). The in-plane AMR is consistent with the traditional AMR theory when the temperature is lower than 25 K, but it is contrary to the traditional AMR principle at higher temperatures.

DATA AVAILABILITY STATEMENT

The original contributions presented in the study are included in the article/Supplementary Material, further inquiries can be directed to the corresponding author.

AUTHOR CONTRIBUTIONS

All authors listed have made significant contributions to the experimental developments, data acquisition, results interpretation, and manuscript writing.

FUNDING

This project was financially supported by the National Science Foundation of China (Grant No.61904205, 12174451, 62174051, 12074437 and 11674400), the Natural Science Foundation of Hunan Province (Grant No. 2020JJ4677), and the Fundamental Research Funds for the Central Universities of Central South University (Grant No. 2020zzts378). The project was also supported by the State Key Laboratory of Powder Metallurgy, Central South University, Changsha, China.

REFERENCES

1. Gong C, Li L, Li Z, Ji H, Stern A, Xia Y, et al. Discovery of intrinsic ferromagnetism in two-dimensional van der Waals crystals. *Nature* (2017) 546:265–9. doi:10.1038/nature22060
2. Huang B, Clark G, Navarro-Moratalla E, Klein DR, Cheng R, Seyler KL, et al. Layer-dependent ferromagnetism in a van der Waals crystal down to the monolayer limit. *Nature* (2017) 546:270–3. doi:10.1038/nature22391
3. Baltz V, Manchon A, Tsoi M, Moriyama T, Ono T, Tserkovnyak Y. Antiferromagnetic Spintronics. *Rev Mod Phys* (2018) 90:15005. doi:10.1103/RevModPhys.90.015005
4. Gong C, Zhang X. Two-dimensional Magnetic Crystals and Emergent Heterostructure Devices. *Science* (2019) 363:706–16. doi:10.1126/science.aav4450
5. Shao Y, Lv W, Guo J, Qi B, Lv W, Li S, et al. The current modulation of anomalous Hall effect in van der Waals Fe3GeTe2/WTe2 heterostructures. *Appl Phys Lett* (2020) 116:092401. doi:10.1063/1.5143323
6. Guo J-j., Xia Q-l., Wang X-g., Nie Y-z., Xiong R, Guo G-h. Temperature and Thickness Dependent Magnetization Reversal in 2D Layered Ferromagnetic Material Fe3GeTe2. *J Magnetism Magn Mater* (2021) 527:167719. doi:10.1016/j.jmmm.2020.167719
7. Wang Y-P, Chen X-Y, Long M-Q. Modifications of Magnetic Anisotropy of Fe3GeTe2 by the Electric Field Effect. *Appl Phys Lett* (2020) 116:092404. doi:10.1063/1.5144032
8. Chen W, Zhang J-m., Nie Y-z., Xia Q-l., Guo G-h. Tuning Magnetic Properties of Single-Layer MnTe2 via Strain Engineering. *J Phys Chem Sol* (2020) 143:109489. doi:10.1016/j.jpcs.2020.109489
9. Zhang J-m., Nie Y-z., Xia Q-l., Xiong R, Guo G-h. Electronic Structures and Magnetic Properties of CrSiTe3 Single-Layer Nanoribbons. *Phys Lett A* (2019) 383:2346–51. doi:10.1016/j.physleta.2019.04.049
10. Xiang Y, Xia Q-l., Luo J-h., Liu Y-p., Peng Y-d., Wang D-w., et al. Observation of Ferromagnetism in Black Phosphorus Nanosheets with High Magnetization by Liquid Exfoliation. *Solid State Commun* (2018) 281:1–5. doi:10.1016/j.ssc.2018.06.008
11. Luo J-h., Li B, Zhang J-m., Zhong M-z., Xia Q-l., Nie Y-z., et al. Bi Doping-Induced Ferromagnetism of Layered Material SnSe2 with Extremely Large Coercivity. *J Magnetism Magn Mater* (2019) 486:165269. doi:10.1016/j.jmmm.2019.165269
12. Tang S, Fishman RS, Okamoto S, Yi J, Zou Q, Fu M, et al. Tuning Magnetic Soliton Phase via Dimensional Confinement in Exfoliated 2D Cr1/3NbS2 Thin Flakes. *Nano Lett* (2018) 18:4023–8. doi:10.1021/acs.nanolett.8b01546
13. Nie Y, Rahman M, Liu P, Sidike A, Xia Q, Guo G-h. Room-temperature Half-Metallicity in Monolayer Honeycomb Structures of Group-V Binary Compounds with Carrier Doping. *Phys Rev B* (2017) 96:075401. doi:10.1103/PhysRevB.96.075401
14. McGuire T, Potter R. Anisotropic Magnetoresistance in Ferromagnetic 3d Alloys. *IEEE Trans Magn* (1975) 11:1018–38. doi:10.1109/TMAG.1975.1058782
15. Thomson W. XIX. On the Electro-Dynamic Qualities of Metals:-Effects of Magnetization on the Electric Conductivity of Nickel and of Iron. *Proc R Soc Lond* (1857) 8:546–50. doi:10.1098/rspl.1856.0144
16. Tumanski S. *Thin Film Magnetoresistive Sensors*, 96. Institute of Physics (2001). Boca Raton: CRC. p. 214. doi:10.1201/9781420033243
17. Wang XR. A Theory for Anisotropic Magnetoresistance in Materials with Two Vector Order Parameters. *Chin Phys. Lett.* (2022) 39:027301. doi:10.1088/0256-307X/39/2/027301
18. Zhang Y, Wang XR, Zhang HW. Extraordinary Galvanomagnetic Effects in Polycrystalline Magnetic Films. *EPL* (2016) 113:47003. doi:10.1209/0295-5075/113/47003
19. Nickel J. *Magnetoresistance Overview*. Palo Alto: Hewlett-Packard Company (1995).
20. Hu J, Liu X, Yue CL, Liu JY, Zhu HW, He JB, et al. Enhanced Electron Coherence in Atomically Thin Nb3SiTe6. *Nat Phys* (2015) 11:471–6. doi:10.1038/nphys3321
21. Li H, He H, Lu H-Z, Zhang H, Liu H, Ma R, et al. Negative Magnetoresistance in Dirac Semimetal Cd3As2. *Nat Commun* (2016) 7:10301. doi:10.1038/ncomms10301
22. Li P, Wen Y, He X, Zhang Q, Xia C, Yu Z-M, et al. Evidence for Topological Type-II Weyl Semimetal WTe2. *Nat Commun* (2017) 8:2150. doi:10.1038/s41467-017-02237-1
23. Wang J, Deng J, Liang X, Gao G, Ying T, Tian S, et al. Spin-flip-driven Giant Magnetotransport in A-type Antiferromagnet NaCrTe2. *Phys Rev Mater* (2021) 5:L091401. doi:10.1103/PhysRevMaterials.5

24. Li J, Badding ME, DiSalvo FJ. New Layered Ternary Niobium Tellurides: Synthesis, Structure, and Properties of Niobium Metal telluride, NbMTe2 (M = Iron, Cobalt). *Inorg Chem* (1992) 31:1050–4. doi:10.1021/ic00032a024
25. Zhang JH, Chen F, Li J, O'Connor CJ. Magnetic Property of Layered Compound NbFeTe2. *J Appl Phys* (1997) 81:5283–5. doi:10.1063/1.364533
26. Bai W, Hu Z, Wang S, Hua Y, Sun Z, Xiao C, et al. Intrinsic Negative Magnetoresistance in Van Der Waals FeNbTe 2 Single Crystals. *Adv Mater* (2019) 31:1900246. doi:10.1002/adma.201900246
27. Bedanta S, Kleemann W. Supermagnetism. *J Phys D: Appl Phys* (2009) 42:013001. doi:10.1088/0022-3727/42/1/013001
28. Gu H, Zhang X, Wei H, Huang Y, Wei S, Guo Z. An Overview of the Magnetoresistance Phenomenon in Molecular Systems. *Chem Soc Rev* (2013) 42:5907–43. doi:10.1039/C3CS60074B

Conflict of Interest: The authors declare that the research was conducted in the absence of any commercial or financial relationships that could be construed as a potential conflict of interest.

Publisher's Note: All claims expressed in this article are solely those of the authors and do not necessarily represent those of their affiliated organizations, or those of the publisher, the editors, and the reviewers. Any product that may be evaluated in this article, or claim that may be made by its manufacturer, is not guaranteed or endorsed by the publisher.